Earthquake rupture in fault zones with along-strike material heterogeneity

Yihe Huang[1]

[1] Department of Earth and Environmental Sciences, University of Michigan.

Corresponding author: Yihe Huang (yiheh@umich.edu)

Key Points:

- Rupture nucleated in a damaged fault zone tends to terminate when it propagates along strike to an intact zone for uniform fault stresses.

- Rupture tends to penetrate into the relatively intact zone when the damaged fault zone becomes wider, sharper and more damaged.

- An asperity at the edge of the relatively intact zone can facilitate rupture when its size is comparable to the nucleation half-length.

Abstract

Geological and geophysical observations reveal along-strike fault zone heterogeneity on major strike-slip faults, which can play a significant role in earthquake rupture propagation and termination. I present 2D dynamic rupture simulations to demonstrate rupture characteristics in such heterogeneous fault zone structure. The modeled rupture is nucleated in a damaged fault zone and propagates on a preexisting fault towards the zone of intact rocks. There is an intermediate range of nucleation lengths that only allow rupture to spontaneously propagate in the damaged fault zone but not in a homogeneous medium given the same stresses and frictional parameters. Rupture with an intermediate nucleation length tends to stop when it reaches the zone of intact rocks for uniform fault stress conditions, especially when the rupture propagation distance in the damaged fault zone is relatively short and when the damaged fault zone is relatively narrow or smooth in the fault-normal direction. Pronounced small-scale heterogeneity within the damaged fault zone also contributes to such early rupture termination. In asymmetric fault zones bisected by a bimaterial fault, rupture moving in the direction of slip of faster rocks tends to terminate under the same conditions as in symmetric fault zones, whereas rupture moving in the direction of slip of slower rocks can penetrate into the zone of intact rocks. A sufficiently-large asperity located at the edge of the zone of intact rocks also allows break-through rupture. The results suggest the along-strike fault zone heterogeneity can play a critical role in seismicity distribution.

Plain language summary

Natural faults are surrounded by a zone of deformed rocks to accommodate strain localization. Such fault zone is not continuous along the fault, but rather includes segments of relatively damaged rocks adjacent to segments of relatively intact rocks. By simulating the dynamic interactions between fault stress, friction and fault zone heterogeneities during the earthquake

rupture process, I show that rupture is more likely to spontaneously propagate inside the damaged fault zone and stop when it reaches the relatively intact zone for uniform fault stress conditions. This phenomenon is less pronounced when the damaged fault zone becomes wider, sharper and more damaged, indicating a higher likelihood of having large earthquakes that can penetrate into the relatively intact zone on more mature faults. The results suggest a priori knowledge of the fault zone heterogeneity is critical for understanding the spatial distribution of earthquakes and the likelihood of having large earthquakes.

1. Introduction

The number of earthquakes generally shows a rapid decay away from the major fault (Power & Jordan, 2010), indicating a concentration of seismicity in the so-called fault zone structure (Ben-Zion & Sammis, 2003). Studies on exhumed faults (e.g., Chester et al., 1993) reveal a hierarchic fault zone structure containing an ultracataclasite layer (centimeters thick), a foliated cataclasite zone (meters thick), and a zone of damaged rocks (10's to 100's meters thick). The fault zone damage can be generated by both the coseismic off-fault damage (Rice et al., 2005) and the long-term fault growth processes including microfracture coalescence, linking of structures, continued displacement on "wavy" faults, and strain localization in a process zone (Mitchell & Faulkner, 2009; Faulkner et al., 2011). Around major strike-slip faults, the ~100-400 meter-wide damaged fault zones are commonly observed from seismic data analysis and distinguish themselves from host rocks by exhibiting much lower seismic velocities, i.e., ~10%-60% for both compressional and shear waves (table 1 in Huang et al., 2014). The widths of damaged fault zones defined by the distances at which fracture density falls to the local background level are found to be in a similar range as the widths of seismically detected fault zones when fault displacement is more than 150 m (Savage & Brodsky, 2009). Damaged fault zones can induce multiple reflection and refraction of seismic waves and modulate dynamic fault stresses during earthquake rupture processes, leading to rupture characteristics such as short rise-time slip pulse (Harris & Day,

1997, Huang & Ampuero, 2011, Pelties et al., 2015), oscillations of rupture speed (Huang et al., 2014), supershear rupture (Ma & Elbanna, 2015; Huang et al., 2016; Albertini & Kammer, 2017), amplified ground motion (Spudich & Olsen, 2001), and enhanced rupture extent (Weng et al., 2016).

It has become common practice to model the damaged fault zone as a uniform low-velocity layer along the fault. In reality, however, it should exhibit along-strike variation of near-fault rock properties, partially because fault zone segments that host earthquakes more frequently are also likely to be more damaged. By defining "structural maturity" based on fault slip, slip rate, age and length, Perrin et al. (2016) showed for 27 large continental earthquakes that the largest earthquake slip on each fault occurred on fault sections with the most compliant rocks. The interseismic velocity fields measured from northern San Andreas fault also suggested highly variable fault zone structure along strike (Chen & Freymueller, 2002; Jolivet et al., 2009; Materna & Burgmann, 2016). Damaged fault zones were observed at Lake San Andreas and Bodega Bay, but not at Black Mountain and Point Reyes that are 30-40 km south, respectively, indicating the critical roles of fault lithology and tectonic setting in sustaining fault zone damage in addition to cumulative displacement (Materna & Burgmann, 2016). It also implies the along-strike variation in fault zone rock properties is likely a common feature on major strike-slip faults where the lithology and tectonic setting vary along strike.

Besides geological and geodetic measurements, seismic observations also support along-strike variation of fault zone structure on major strike-slip faults. Lewis and Ben-Zion (2010) found the coherency of fault zone trapped waves breaks down at a distance interval of 3-5 km along the ~40 km long Parkfield section of the San Andreas fault, suggesting a highly heterogeneous fault zone along strike. More detailed observations come from 5 dense seismic arrays across the Anza seismic gap in the San Jacinto fault, a 20-km segment devoid of active seismicity (Sanders & Kanamori, 1984), and across the southern section of the Clark branch south of the Anza gap

where abundant seismicity was clustered. Yang et al. (2014) detected damaged fault zones within the Anza gap and south of the Anza gap, but not near the two ends of the Anza gap. A similar relationship between the spatial distribution of small earthquakes and damaged fault zones has also been observed in an oceanic setting, along the Discovery transform fault, East Pacific Rise (Froment et al., 2014; Wolfson-Schwehr et al., 2014).

Why seismicity tends to cluster inside damaged fault zones and stay away from rupturing into zones of intact rocks remains an intriguing question. Theoretically speaking, in order for earthquake rupture to be nucleated successfully, its nucleation length needs to be larger than a certain threshold, i.e., critical nucleation length, which is proportional to the shear moduli of near-fault rocks (e.g., Andrews, 1976a, 1976b; Uenishi & Rice, 2003; Day et al., 2005; Galis et al., 2014). Hence, given the same fault stress conditions, earthquakes in damaged fault zones have smaller critical nucleation patches than those in relatively intact zones. It means earthquakes would prefer rupturing within damaged fault zones and may stop once they reach relatively intact zones when stresses are nearly uniform along the fault. This may explain why the relatively intact zones near the ends of the Anza gap can act as barriers for earthquakes nucleated in the damaged fault zones outside the Anza gap. A further question is when rupture may break through such material barriers and result in large earthquakes.

The goal of this paper is to elucidate the effects of the along-strike variation of fault zone structure on inducing earthquake rupture termination and investigate the conditions that cause rupture to break through such material barriers for both uniform and heterogeneous fault stress conditions using 2D dynamic rupture models. I simplify the heterogeneous fault zone structure as a preexisting damaged fault zone adjacent to a zone of intact rocks in the along-strike direction and simulate dynamic rupture nucleated inside the preexisting damaged fault zone (Figure 1). The model parameter space includes the rupture nucleation length, rupture propagation distance in the damaged fault zone, damaged fault zone width and velocity, fault zone structure

smoothness and asymmetry, and stress heterogeneity along the fault. I describe the model assumptions and setup in section 2 and present how the model parameters can affect rupture termination and penetration in section 3. I discuss the application of the simulation results to realistic scenarios and the possible interplay between the fault zone heterogeneity and other fault complexities in section 4.

2. Model setup

The damaged fault zone is modeled as an elastic low-velocity layer bisected by a planar preexisting fault, which extends through the zone of intact rocks (Figure 1). The compressional and shear wave velocities are reduced by the same fraction in damaged fault zones. Earthquake rupture is nucleated inside the damaged fault zone and modeled as 2D dynamic in-plane rupture, which can represent the along-strike rupture on a vertical strike-slip fault that is infinitely long along dip. Material properties of the damaged fault zone can be either symmetric or asymmetric across the fault. In symmetric fault zones, seismic velocities can decrease either abruptly or smoothly from host rocks to the fault zone. I name these two scenarios sharp fault zone (Figure 2a) and smooth fault zone (Figure 2b), respectively. Smooth fault zones may better characterize the shallow parts of damaged fault zones due to low confining stresses there. For example, borehole data from the Nojima fault zone at ~630 m depth shows an exponential decay of seismic wave velocities from host rocks to the fault zone (Huang & Ampuero, 2011), whereas borehole data from the San Andreas fault zone at ~3 km depth exhibits a sharp reduction of seismic wave velocities within the damaged fault zone (Zoback et al., 2011). I describe smooth fault zones using a Gaussian distribution of seismic wave velocities: $v(z) = v_0 - \Delta v e^{-z/l_z}$, where v_0 is the seismic velocity of the host rock, Δv is the velocity contrast, z is the fault-normal distance from the fault, and l_z is half of the characteristic fault zone width where 63% of the velocity contrast is achieved. I also consider the small-scale variation of seismic wave velocities along strike within the damaged fault zone and name this scenario rough fault zone (Figure 2c).

The small-scale material heterogeneity is described by the characteristic length scale l_x and the roughness α: $v(z) = v_0 - \Delta v e^{-z/(l_z(1-\alpha\cos(\frac{x}{l_x})))}$. Such spatially periodic pattern of damage may result from rupture with oscillating rupture speeds in damaged fault zones with off-fault plasticity (Huang et al., 2014). The fault zone damage changes more abruptly as α increases, and $\alpha < 1$ for a fault zone that is continuously damaged along strike. The fourth type of the damaged fault zone is an asymmetric fault zone with contrasting seismic velocities on two sides of the fault (Figure 2d).

In the symmetric fault zone, I apply a linear slip-weakening friction law to the fault to characterize the drop from the static friction μ_s to the dynamic friction μ_d when fault slip reaches the critical slip distance D_c (Andrews, 1976a, 1976b). Initial shear stresses τ_0 and normal stresses σ_0 are uniform outside the nucleation zone except in section 3.4. This uniform stress condition is considered as an end member of the realistic stress conditions on mature faults. The other end member is the uniform strain condition caused by a constant far-field loading. The uniform strain condition results in higher shear stresses in the relatively intact zone, which can facilitate rupture propagation in as shown in section 3.4. I also compare the results from anti-plane rupture for both uniform stress and uniform strain conditions in the discussion section. Fully dynamic earthquake cycle simulations are needed to incorporate more realistic stress conditions that evolve temporarily and spatially (Lapusta et al., 2000; Kaneko et al., 2011; Thakur and Huang, 2018). I choose an initial shear stress that is equivalent to an S ratio of 3, where $S = (\mu_s\sigma_0 - \tau_0)/(\tau_0 - \mu_d\sigma_0)$ (Das & Aki, 1977), to represent averagely low stress state on mature faults (Rice, 1992; Noda et al., 2009). Given the same static ($\mu_s\sigma_0$) and dynamic shear strengths ($\mu_d\sigma_0$), S ratio decreases as the initial shear stress increases. High shear stresses (S <1.77) can cause supershear transition in a 2D homogeneous medium (Andrews, 1985). Supershear rupture can occur in damaged fault zones at even lower shear stress conditions than in a homogeneous medium (Huang et al., 2016).

In the asymmetric fault zone, because dissimilar fault zone materials induce a normal stress perturbation during rupture propagation, I require the normal stress to continuously evolve with time to avoid unstable results caused by an instantaneous stress change (Cochard & Rice, 2000; Rubin & Ampuero, 2007; Ampuero & Ben-Zion, 2008): $\frac{d\sigma^*}{dt} = \frac{V^*}{D_\sigma}(\sigma - \sigma^*)$, where σ^* is the effective normal stress relevant to the surface strength, V^* is the reference slip rate, and D_σ is the reference distance. The pure temporal dependence ensures that simulations are well resolved for large slip rates but may have the disadvantage of generating noisy stopping phases (Rubin & Ampuero, 2007). The values of V^* and D_σ are shown in Table 1. D_σ is chosen to be much smaller than the critical slip distance D_c to maintain a strong bimaterial effect.

To successfully nucleate the rupture, I apply an initial shear stress that is ~ 0.01% higher than the static shear strength within the nucleation zone (Figure 1). Since the critical nucleation length is proportional to the shear modulus of near-fault rocks G (e.g., Andrews, 1976a, 1976b; Uenishi & Rice, 2003; Day et al, 2005; Galis et al., 2015), the critical nucleation length in a homogenous medium is ~4 times as large as that in a very wide damaged fault zone with 50% velocity reduction given the same stress conditions and frictional parameters. When the fault zone width is comparable to the nucleation length, a combination of the shear moduli of the fault zone rocks and host rocks should be used to calculate the critical nucleation length. Note that different estimates of the critical nucleation length are derived due to various model assumptions (Galis et al., 2015). The critical nucleation length also depends on the initial shear stress conditions when it is determined from the crack tip energy balance under the assumption of uniform stress drop (Andrews, 1976a, 1976b; Day et al, 2005). But it is only controlled by the shear modulus and frictional parameters for mode II slip-weakening rupture in a homogeneous medium when there is a localized and gradually increasing stress loading (Uenishi & Rice, 2003). Galis et al. (2015) solves the critical nucleation area using 3D dynamic rupture simulations with an overstressed patch, which is the 3D counterpart of our model setup. Their estimates of the critical nucleation area are not sensitive to initial shear conditions when the S ratio is less than 0.75, but increase

with S ratios when the S ratio is larger than 0.75. Compared to an overstressed nucleation patch, a time-weakening nucleation zone within which the frictional strength is gradually reduced (Andrews, 1985) requires larger nucleation lengths for successful nucleation, but both kinds of nucleation procedures produce similar characteristics of spontaneous rupture outside the nucleation zone.

The dynamic rupture is calculated using a 2D spectral element method (SEM2DPACK, http://www.sourceforge.net/projects/sem2d/). I require 5 GLL nodes per element side and choose an element size that is small enough to resolve the reduction from the static friction to the dynamic friction in the rupture process zone. I also use dimensionless quantities (Table 1) to facilitate the comparison between simulation results and rupture scenarios with realistic fault zone properties. The spatial dimension is normalized by $L_c = G^{HOST} D_c / \sigma_0 (\mu_s - \mu_d)$, a characteristic length scale of the rupture process zone introduced by the slip-weakening process (e.g., Dunham 2007). As demonstrated further in section 3.1, the critical nucleation half-length in a homogeneous medium is $\sim 0.8\, L_c$ given the parameters used in this study. The temporal dimension is normalized by $t_c = L_c / v_s^{HOST}$, where v_s^{HOST} is the shear wave velocity of the host rock. Slip is normalized by the critical slip distance D_c. Stresses are normalized by the strength drop $\Delta \tau_s = \sigma_0 (\mu_s - \mu_d)$, i.e., the difference between the static and dynamic shear strengths.

Table 1. Model parameters

Dimensionless quantity	Symbol	Value
Density	ρ	1
Shear modulus of the host rock	G^{HOST}	1
Shear wave velocity of the host rock	v_s^{HOST}	1
Compressional wave velocity of the host rock	v_p^{HOST}	$\sqrt{3}$
Initial shear stress	τ_0	0.45

Normal stress	σ_0	2
Static friction coefficient	μ_s	0.6
Dynamic friction coefficient	μ_d	0.1
Critical slip distance	D_c	1
Reference slip rate on the bimaterial fault	V^*	1
Reference distance on the bimaterial fault	D_σ	0.2

3. Results

3.1 The effect of rupture propagation distance in damaged fault zones

I first compare the characteristics of rupture with different nucleation lengths in a homogeneous medium and in a 1 L_c wide sharp fault zone with 50% velocity reduction. I find an intermediate range of nucleation half-lengths ($\sim$0.35-0.8 L_c) that allow rupture to propagate in the damaged fault zone but not in a homogeneous medium. The upper bound is very close to the critical nucleation half-length of mode II slip-weakening rupture in a homogeneous medium when there is a localized and gradually increasing stress loading (Uenishi & Rice, 2003). The lower bound would decrease and approach the theoretical prediction (0.2 L_c) as the fault zone width increases to infinity. I expect earthquakes on mature faults with low shear stress levels to have nearly-critical nucleation lengths, but faults with high shear stress levels, which may be manifested by the occurrence of energetic events with high stress drop (Baltay et al., 2011), can lead to larger nucleation lengths and thus more energy available for rupture propagation. Similar to the results from previous dynamic rupture simulations (Huang & Ampuero, 2011; Huang et al., 2014), rupture in the damaged fault zone propagates as short rise-time slip pulses followed by long cracks due to the reflections of compressional and shear waves, whereas rupture in the homogeneous medium exhibits long cracks with lower peak slip rate than rupture in the damaged fault zone (Figure 3). Rupture speeds approach the Rayleigh wave speeds of the damaged fault zone and the homogeneous medium, respectively.

I introduce the along-strike variation of near-fault rock properties in the following simulations. Rupture is nucleated within an intermediate nucleation patch in a damaged fault zone and propagates towards a zone of intact rocks outside the damaged fault zone. The most pronounced effect of the along-strike fault zone segmentation is rupture termination at the ends of the damaged fault zone. Figure 4a demonstrates an abrupt stopping phase when rupture reaches the zone of intact rocks. Since rupture already became spontaneous and approached the fault zone Rayleigh wave speed, the stopping phase is caused by the change of near-fault rock properties rather than an unsuccessful nucleation. Rupture termination generates a back-propagating rupture front and radiates high-frequency waves at the ends of the damaged fault zone. The final rupture size is $4\,L_c$ for a unilateral rupture or $8\,L_c$ for a bilateral rupture. Because the damaged fault zone has a width of $1\,L_c$ in the simulation and the fault zone widths are ~100-400 m for major strike-slip faults (table 1 in Huang et al., 2014), L_c is also in the order of 100 m, and a rupture size of 4-8 L_c corresponds to a magnitude ~4-5 earthquake on these faults. Rupture would also terminate earlier if other stress, frictional or geometric barriers were present within the damaged fault zone.

Whether rupture stops as it reaches the zone of intact rocks also depends on the along-strike distance from the hypocenter to the zone of intact rocks. Rupture that propagates in the damaged fault zone for a sufficiently long distance is more likely to penetrate into the zone of intact rocks and continue propagating afterwards, because it tends to carry larger dynamic stresses ahead of the rupture front and thus have more energy available for rupture propagation before reaching the zone of intact rocks (Figure 4b). A further analysis of the balance between the energy release rate and fracture energy (e.g., Tada et al., 2000; Kammer et al., 2015; Bayart et al., 2016) will help understand the change of the energy release rate near the end of the damaged fault zone for different rupture propagation distances. The penetration of rupture causes an abrupt reduction of the rupture speed followed by its rapid growth. After the initial rupture speed oscillations, it approaches the Rayleigh wave speed in a homogeneous medium. There is also a transition of

rupture characteristics from "skinny" slip pulses with large slip rate in the damaged fault zone to "fat" cracks with low slip rate in the zone of intact rocks, suggesting a domination of high-frequency ground motions earlier but relatively long-period ground motions later. The resulting slip is the highest in the damaged fault zone and decreases in the zone of intact rocks.

3.2 The effects of damaged fault zone width, velocity and smoothness

As damaged fault zones become wider, rupture nucleation becomes more sensitive to the lower shear moduli of near-fault rocks, leading to a shorter critical nucleation length. The same trend of the critical nucleation length also applies to more damaged fault zones. Thus, rupture nucleated in wider or more damaged fault zones is more likely to penetrate into the zone of intact rocks given the same nucleation patch (the blue dashed line in Figure 5). For example, in a 1 L_c wide fault zone with 50% velocity reduction, the size of nearly-critical unilateral rupture with a nucleation half-length of 0.4 L_c can hardly exceed ~6 L_c, i.e., less than 1 km when L_c is in the order of 100 m. But rupture that propagates for a distance of 6 L_c can penetrate into the zone of intact rocks when the damaged fault zone is 2 L_c wide. A similar rupture behavior holds true for a 1 L_c wide fault zone with 60% velocity reduction. Note that since the damaged fault zone width is normalized by L_c, a certain damaged fault zone can be considered either narrow or wide for rupture with different critical nucleation lengths in a homogeneous medium.

In contrast to rupture in sharp fault zones, rupture in smooth fault zones with identical fault rock properties tend to terminate more frequently when their characteristic widths are the same as the widths of sharp fault zones (the yellow dashed line in Figure 5). This is because the average shear modulus of near-fault rocks in smooth fault zones is larger than that in sharp fault zones with the same widths (Figure 2b), resulting in a longer critical nucleation length. Such variation of rupture characteristics with fault zone structure indicates the correlation between large earthquakes and mature fault zones. The damaged fault zone may be more distributed at a young

stage when multiple fault strands help accommodate deformation and become more concentrated and established as it matures (Perrin et al., 2016). A proxy for this maturation process is the evolution from a smooth and less damaged fault zone to a sharp and more damaged fault zone. Hence, the barrier effect of the along-strike fault zone heterogeneity would be stronger when the damaged fault zone was relatively young. As the damaged fault zone becomes more damaged and sharper, there is a higher likelihood of having large earthquakes that can penetrate into the relatively intact zone. Since the shallow parts of damaged fault zones tend to be smoother, this barrier mechanism may also contribute to the termination of earthquake rupture when it propagates to free surface.

Both sharp and smooth fault zones are ideal cases that have uniformly damaged rocks along strike within the fault zones. However, the small-scale variation of rock properties within damaged fault zones could be a prominent feature especially when the fault zone structure is developing. I investigate how the roughness of the damaged fault zone α (Figure 2c) affects the conditions leading to rupture termination. I find that rupture can propagate through damaged fault zones with pronounced small-scale damage variation ($\alpha = 0.5$), but it tends to terminate when approaching the zone of intact rocks (Figure 6a). As the roughness α decreases, rupture is more likely to penetrate into the zone of intact rocks (Figure 6b). In contrast to break-through rupture for the case of sharp fault zones, break-through rupture for the cases of smooth and rough fault zones accelerates gradually after the initial rupture speed reduction without any rupture speed oscillations in the zone of intact rocks.

3.3 The effects of asymmetric fault zones

Faults can be surrounded by dissimilar rocks in certain tectonic settings, especially when continental and oceanic rocks are in contact. These so-called bimaterial faults have been found in major strike-slip fault zones such as North Anatolian fault (e.g., Najdahmadi et al., 2016), San

Andreas fault (e.g., Dor et al., 2006; Share & Ben-Zion, 2016) and Hayward fault (e.g., Allam et al., 2014). To understand the effects of bimaterial faults on rupture termination, I model rupture in an asymmetric fault zone with different rock properties on two sides of the fault. I choose a 50% velocity contrast on one side and a 40% velocity contrast on the other side, so the velocity contrasts on both sides fall in the range of the observed material properties of major strike-slip fault zones (Figure 2d). It also ensures the existence of the generalized Rayleigh speed, which only occurs when one side is less than 35.9% faster than the other side (Harris & Day, 1997; Rubin & Ampuero, 2007).

I find the rupture front moving in the direction of slip of faster rocks along the bimaterial fault (to the left in Figures 2d and 7a) stops propagating under the same conditions as rupture in the symmetric fault zone. The rupture front moving in the direction of slip of slower rocks (to the right in Figures 2d and 7a), however, has larger slip rate and can penetrate into the zone of intact rocks after the rupture front moving in the opposite direction already stops. Rupture fronts moving in both directions can penetrate into the zone of intact rocks when they propagate in the damaged fault zone for longer distances (Figure 7b). In this case, the rupture front moving in the direction of slip of slower rocks reaches a further distance due to the faster rupture speed. The seismogenic fault in the Clark section of the San Jacinto fault zone is inferred to be located near the western edge of a damaged fault zone, and thus near-fault rocks are slower on the northeast side of the seismogenic fault (Qiu et al., 2017). Earthquake rupture nucleated in such an asymmetric fault zone south of the Anza gap would encounter more barrier effects when it propagates to the northwest and reaches the relatively intact zone at the southern end of the Anza gap. It suggests the concentration of small earthquakes south of the Anza gap may result from the combined effects of the along-strike variation of near-fault rock properties and the asymmetry of damaged fault zone structure.

3.4 The effects of heterogeneous shear stresses

Shear stresses on natural faults are heterogeneous in various spatial scales (Smith & Heaton, 2010) partially due to the change of fault geometry and frictional properties. For example, fault surface roughness can exist at scales ranging from 10^{-5} to 10 m (Candela et al., 2012) and introduce high stress asperities on extensional fault bends. Moreover, as small earthquakes release shear stresses in the damaged fault zone more frequently, shear stresses in the zone of intact rocks can be higher than those in the damaged fault zone after a period of stress accumulation. Eventually shear stresses in the zone of intact rocks will be accumulated to such a high level that allows rupture to break through. To investigate shear stress conditions required for rupture to penetrate into the zone of intact rocks, I gradually increase the level of initial shear stresses in the zone of intact rocks while keeping the other model parameters the same in each simulation. I find rupture can only penetrate into the zone of intact rocks that is 6 L_c away from the hypocenter when the dynamic stress drop (i.e., the difference between the initial shear stress and the dynamic shear strength) in the zone of intact rocks is not less than 28% higher than the dynamic stress drop in the damaged fault zone (Figure 8a). It means when the damaged fault zone and the zone of intact rocks have the same dynamic shear strengths, shear stresses in the zone of intact rocks should be at least ~0.84 MPa higher than that in the damaged fault zone to allow rupture to break through if the dynamic stress drop is 3 MPa in the damaged fault zone.

The other extreme case is a high-stress patch, i.e., an asperity, located at the edge of the zone of intact rocks. Such high stress asperities may result from localized stress accumulation in the gap between the rupture areas of previous earthquakes. The size of the asperity required for break-through rupture could be much smaller than the along-strike dimension of the zone of intact rocks, provided sufficiently high shear stresses in the asperity. Moreover, shear stresses in the asperity should be less than a certain threshold, above which an earthquake may prefer rupturing in the asperity first. I deliberately choose an initial shear stress level that corresponds to $S = 1.86$ in the asperity, slightly lower than the shear stress level allowing supershear rupture in a

homogeneous medium ($S < 1.77$). I then gradually increase the asperity size in each simulation to find the threshold that overcomes the barrier effects of the intact rocks. For nearly-critical rupture, it is when the asperity size gets close to or larger than the nucleation half-length that earthquake rupture can penetrate into the zone of intact rocks. For example, rupture with a nucleation half-length of 0.4 L_c can penetrate into the zone of intact rocks that is 6 L_c away from the hypocenter when the high-stress asperity is larger than 0.35 L_c (Figure 8b).

4. Discussion

The motivation of this study was to provide a plausible explanation for the correlation between the along-strike distribution of small-to-moderate earthquakes and damaged fault zones. The results suggest that the along-strike variation of rock properties along the San Jacinto fault zone may induce the termination of earthquake rupture when it propagates to the relatively intact zone near the end of the Anza gap and cause the concentration of seismicity south of the Anza gap. In reality, the along-strike fault zone heterogeneity may vary from more damaged fault zones to less damaged fault zones instead of zones of intact rocks. Given the critical nucleation length of rupture in more damaged fault zones is smaller than that in less damaged fault zones, we should still expect a concentration of seismicity in more damaged segments and occasional penetration of earthquake rupture into less damaged segments. It is also possible for earthquakes to be nucleated within the relatively intact zones if fault friction or shear stresses there are more favorable for rupture nucleation. For example, in the case of Figure 8b, rupture would be nucleated within the asperity if the local shear stress reached the static shear strength of the intact rocks. The resulting rupture may not propagate into the damaged fault zones if small earthquakes have already released all the stress budget there. This scenario may explain the abundant microseismicity within the highly damaged fault segment and the occurrence of magnitude 6 earthquakes in the relatively intact fault segment along the Gofar oceanic transform fault (Froment et al., 2014). On the other hand, if rupture is nucleated in the damaged fault zone and

propagates through the relatively intact zone, we should observe a nearly triangular slip profile with its peak in the damaged fault zone and decreasing slip in the relatively intact zone, which is consistent with the generic earthquake slip profile (Cappa et al., 2014).

This study can be applied to a wide range of spatial scales given the spatial dimensions are normalized by the characteristic length scale L_c in the simulations. The barrier effect of the relatively intact zone is most pronounced when the rupture nucleation length is comparable to the fault zone width (Figure 5). For unilateral rupture that propagates spontaneously in a 1 L_c wide damaged fault zone with 50% velocity reduction, the lower bound of the rupture length within the damaged fault zone is the critical nucleation half-length, i.e., ~0.35 L_c, and the upper bound is the longest rupture propagation distance in the damaged fault zone for nearly critical rupture, i.e., ~6 L_c (the red dashed line in Figure 5). It means this material barrier effect can contribute to the generation of magnitude ~1 to magnitude ~4 earthquakes that have rupture lengths of ~35 to ~600 m in a 100 m wide fault zone. Note that rupture can be arrested by itself when its nucleation length is less than the critical threshold (Xu et al., 2015), generating even shorter rupture lengths and thus smaller earthquakes than the above-mentioned lower bound. Moreover, the size of the high stress asperity that allows break-through rupture is also scale dependent and comparable to the nucleation half-length. If such asperity exists at the end of the Anza seismic gap, it should be at least several tens of meters long to facilitate rupture penetration into the Anza seismic gap given the San Jacinto fault zone is ~200 m wide (Yang et al., 2014).

Due to the simple model setup, details of rupture characteristics in the simulations can be different from those in real earthquakes. The 2D simulations simplify the damaged fault zone to an elastic low-velocity layer that is infinitely long along dip. It means the simulation results are most applicable to strike-slip earthquakes when their rupture occurs within the damaged fault zone and is not affected by the free surface. Some analyses of fault zone waves suggested damaged fault zones can extend to a depth of ~7-10 km where seismicity is abundant (e.g., Li et

al., 1994; Li et al., 2007), whereas other seismic waveform studies reported shallow fault zones at 2-3 km (e.g., Lewis & Ben-Zion, 2010; Yang & Zhu, 2010). Huang et al. (2016) showed that a damaged fault zone in Big Bear, CA caused a peak at 10-20 Hz in the P-wave spectra of M_w 2.1-3.1 aftershocks, suggesting the damaged fault zone should extend to the depths of these aftershocks (4-6.5 km). Perrin et al. (2016) distinguished the few-hundred-meter wide inner damage zone where rocks are densely fractured from the outer damage zone where more distributed damage occurs. The inner damage zone may reach the bottom of the seismogenic zone, whose depth also provides an upper limit on the damage zone width (Ampuero & Mao, 2017).

Another underlying assumption in the 2D simulations is a uniform distribution of fault zone rock properties along dip, which is inconsistent with the notion of a flower-structure fault zone with decreasing widths and velocity contrasts with depth (e.g., Cochran et al., 2009). For strike-slip earthquakes, the along-dip variation of fault zone structure should have less influence on the along-strike rupture propagation. Pelties et al. (2015) showed in the 3D dynamic rupture simulations that a flower-structure fault zone can induce slip pulses with varying rise time with depth, and the rise time at a given depth agrees with the rise time calculated from 2D rupture simulations using the same velocity contrast and width at that depth. On the other hand, the along-dip variation of fault zone structure should have a significant effect on the along-dip rupture propagation and may prohibit rupture from propagating to the deeper zone of intact rocks, in a similar fashion to the along-strike rupture termination. To test this, I model 2D dynamic anti-plane rupture in damaged fault zones, which better represents the along-dip rupture propagation on a vertical strike-slip fault. The stress conditions and frictional parameters are the same as those for in-plane rupture (Table 1). Similar to in-plane rupture (Figure 4), anti-plane rupture terminates at the ends of damaged fault zone for a relatively short rupture propagation distance in the damaged fault zone, whereas anti-plane rupture that propagates in the damaged fault zone for

a longer distance can penetrate into the intact rocks (Figure 9). Thus, I find anti-plane rupture also shows a dependence on the variation of fault zone properties for a uniform stress condition.

One limitation of dynamic rupture simulations is the assumption of fault stress states in the model setup. I consider a uniform stress condition in the simulations except for section 3.4. The other end member of realistic fault scenarios is a uniform strain condition under the assumption of a constant far-field loading. For a uniform strain condition, anti-plane rupture that is nucleated in a lower half-space and propagates towards the upper layer with a different shear modulus can lead to a discontinuity of stress drops that are proportional to the shear moduli of the adjoining media (Bonafede et al., 2002; Rybicki & Yamashita, 2002). Hence, rupture is more likely to stop if it propagates from a relatively intact zone to a damaged fault zone, due to the much lower stress drop in the damaged fault zone (Kame et al., 2008). However, the effect of the critical nucleation length was not considered in the uniform strain models above. If the critical nucleation length is in dependent of initial shear stress conditions but depends on the shear modulus and frictional parameters, as for a slip-weakening fault under a localized and gradually increasing stress loading (Uenishi & Rice, 2003) and for a rate-and-state fault under a slow tectonic loading (Rice, 1993; Rubin and Ampuero, 2005), rupture is still prone to be nucleated in the damaged fault zone and may terminate more frequently within the fault zone due to its low stress states. More realistic scenarios will require fully dynamic earthquake simulations with fault zone material heterogeneity (Kaneko et al., 2011). Our fully dynamic earthquake cycle simulations showed that seismicity tends to cluster in the shallow damaged fault zone on a vertical strike-slip fault (Thakur & Huang, 2018).

Kinematic rupture properties such as rupture velocity and slip rate also depend on fault friction and stress conditions in the simulations. The relatively low initial shear stresses give rise to slow rupture propagating at the Rayleigh wave speed of the damaged fault zone in this study. Increasing the initial shear stress level in the damaged fault zone will eventually lead to

supershear rupture propagating faster than the shear wave velocity of the host rock. Supershear rupture in damaged fault zones can occur at lower fault stress conditions than in a homogeneous medium and propagate stably at speeds that are considered as unstable for supershear rupture in a homogeneous medium, i.e., between the shear wave velocity and $\sqrt{2}$ of the shear wave velocity of the host rock (Huang et al., 2016). Supershear rupture has been related to the most mature fault sections (Perrin et al., 2016), which can be caused by a combination of damaged fault zones around the mature fault sections and relatively high shear stress conditions.

It is noted that other fault complexities such as the change of fault geometry and frictional behaviors can cause the along-strike segmentation of seismicity as well. In the case of the Gofar transform fault (Froment et al., 2014), the ~600 m offset near the boundary between the relatively intact zone and the damaged fault zone may contribute to the rupture termination of magnitude 6 earthquakes, but it cannot explain the concentration of microseismicity in the damaged fault zone. It has been proposed that the damaged fault zone may give rise to higher porosity and hydrothermal alteration that prevent the damaged fault zone from hosting large earthquakes (Froment et al., 2014). We need to investigate further how fluid flow can affect the ability of the damaged fault zone to host large earthquakes and how it interacts with the barrier effect of the along-strike fault zone heterogeneity, which will be important factors to consider for injection-induced seismicity (Ellsworth, 2013) besides earthquakes on oceanic transform faults. Future efforts will also be directed towards developing more realistic earthquake models that incorporate fault zone damage rheology (e.g., Xu et al., 2014; Thomas et al., 2016), seismicity on secondary fault strands (e.g., Ross et al., 2017) and along-dip variation of fault zone structure, especially on subduction plate boundary faults (e.g., Rowe et al., 2013).

5. Conclusions

The size of an earthquake largely depends on where rupture stops. I show that the along-strike variation of fault zone structure that surrounds major strike-slip faults can contribute significantly to rupture termination for uniform fault stress conditions. This material barrier effect is pronounced for nearly-critical rupture that is nucleated in damaged fault zones and propagates towards relatively intact zones when its nucleation length is comparable to the fault zone width. Break-through rupture is more favorable when damaged fault zones become wider, sharper or more damaged, indicating a higher likelihood of having larger earthquakes on more mature faults. Break-through rupture is also possible when an asperity is located at the edge of the relatively intact zone, but its size needs to be comparable to the rupture nucleation length and its shear stress level needs to be sufficiently higher than that in the damaged fault zone. The results suggest that a priori knowledge of the along-strike variation in near-fault rock properties, which may be related to cumulative displacement, fault lithology, tectonic setting and historical earthquake rupture, is critical in understanding seismicity distribution and the likelihood of having large earthquakes. A detailed comparison between theoretical models described in this paper and seismic observations along major strike-slip faults, particularly those with well-known seismic gaps and at high risk of having large earthquakes, will provide valuable insights into how the along-strike variation of fault zone heterogeneity plays a role in seismicity distribution under various fault conditions.

Acknowledgement

is SCEC contribution #8904. The simulation results are available on UM Deep Blue (https://deepblue.lib.umich.edu/).

References

Albertini, G., & Kammer, D. S. (2017). Off-fault heterogeneities promote supershear transition of dynamic mode II cracks. *Journal of Geophysical Research: Solid Earth*, *122*(8), 6625–6641. https://doi.org/10.1002/2017JB014301

Allam, A.A., Ben-Zion Y., & Peng, Z. (2014). Seismic imaging of a bimaterial interface along the Hayward fault, CA, with fault zone head waves and direct P arrivals. *Pure and Applied Geophysics*, *171*(11), 2993-3011. https://doi.org/10.1007/s00024-014-0784-0

Ampuero, J.-P., & Ben-Zion, Y. (2008). Cracks, pulses and macroscopic asymmetry of dynamic rupture on a biomaterial interface with velocity-weakening friction. *Geophysical Journal International, 173*(2), 674-692. https://doi.org/10.1111/j. 1365-246X.2008.03736.x

Ampuero, J. P., & Mao, X. (2017). Upper limit on damage zone thickness controlled by seismogenic depth. *Fault Zone Dynamic Processes: Evolution of Fault Properties During Seismic Rupture*, 243-253. http://doi.org/10.1002/9781119156895.ch13

Andrews, D.J. (1976a). Rupture propagation with finite stress in antiplane strain, *Journal of Geophysical Research*, *81*(20), 3575–3582. https://doi.org/10.1029/JB081i020p03575

Andrews, D. J. (1976b), Rupture velocity of plane strain shear cracks, *Journal of Geophysical Research*, *81*(32), 5679–5687. https://doi.org/10.1029/JB081i032p05679

Andrews, D.J. (1985). Dynamic plane-strain shear rupture with a slip-weakening friction law calculated by a boundary integral method. *Bulletin of the Seismological Society of America, 75*(1), 1-21.

Bayart, E., Svetlizky, I., & Fineberg, J. (2016). Fracture mechanics determine the lengths of interface ruptures that mediate frictional motion. *Nature Physics, 12*(2), 166. https://doi.org/10.1038/NPHYS3539

Ben-Zion, Y., & Sammis, C.G. (2003). Characterization of fault zones. *Pure and Applied Geophysics*, *160*(3), 677-715. https://doi.org/10.1007/PL00012554

Bonafede, M., Parenti, B., & Rivalta, E. (2002). On strike-slip faulting in layered media. *Geophysical Journal International, 149*(3), 698-723. https://doi.org/10.1046/j.1365-246X.2002.01670.x

Candela, T., Renard, F., Klinger, Y., Mair, K., Schmittbuhl, J., & Brodsky, E. E. (2012). Roughness of fault surfaces over nine decades of length scales. *Journal of Geophysical Research: Solid Earth, 117*(B8). https://doi.org/10.1029/2011JB009041

Cappa, F., Perrin, C., Manighetti, I., & Delor, E. (2014). Off-fault long-term damage: A condition to account for generic, triangular earthquake slip profiles. *Geochemistry, Geophysics, Geosystems, 15*(4), 1476-1493. https://doi.org/10.1002/2013GC005182

Chen, Q., and J. T. Freymueller (2002), Geodetic evidence for a near-fault compliant zone along the San Andreas Fault in the San Francisco Bay Area, Bulletin of the Seismological Society of America, **92**(2), 656–671. https://doi.org/10.1785/0120010110

Chester F.M., Evans, J. P., & Biegel, R. L. (1993). Internal structure and weakening mechanisms of the San Andreas fault. *Journal of Geophysical Research: Solid Earth*, **98**(B1), 771-786. https://doi.org/10.1029/92JB01866

Cochard, A., & Rice, J. R. (2000). Fault rupture between dissimilar materials: Ill-posedness, regularization, and slip-pulse response. *Journal of Geophysical Research: Solid Earth*, **105**(B11), 25891-25907. https://doi.org/10.1029/2000JB900230

Cochran, E. S., Li, Y. G., Shearer, P. M., Barbot, S., Fialko, Y., & Vidale, J. E. (2009). Seismic and geodetic evidence for extensive, long-lived fault damage zones. *Geology*, **37**(4), 315-318. https://doi.org/10.1130/G25306A.1

Das, S., & Aki, K. (1977). A numerical study of two-dimensional spontaneous rupture propagation. *Geophysical journal international*, **50**(3), 643-668. https://doi.org/10.1111/j.1365-246X.1977.tb01339.x

Day, S. M., Dalguer, L. A., Lapusta, N., & Liu, Y. (2005). Comparison of finite difference and boundary integral solutions to three-dimensional spontaneous rupture. *Journal of Geophysical Research: Solid Earth*, **110**, B12307. https://doi.org/10.1029/2005JB003813

Dor, O., Rockwell, T. K., & Ben-Zion, Y. (2006). Geological observations of damage asymmetry in the structure of the San Jacinto, San Andreas and Punchbowl faults in Southern California: a possible indicator for preferred rupture propagation direction. *Pure and Applied Geophysics*, **163**(2-3), 301-349. https://doi.org/10.1007/s0024-005-0023-9

Dunham, E. M. (2007). Conditions governing the occurrence of supershear ruptures under slip-weakening friction. *Journal of Geophysical Research: Solid Earth*, *112*, B07302, https://doi.org/10.1029/2006JB004717

Ellsworth, W. L. (2013). Injection-induced earthquakes. *Science, 341*(6142), 1225942. https://doi.org/10.1126/science.1225942

Faulkner, D. R., Mitchell, T. M., Jensen, E., & Cembrano, J. (2011). Scaling of fault damage zones with displacement and the implications for fault growth processes. *Journal of Geophysical Research: Solid Earth*, *116*, B05403. https://doi.org/10.1029/2010JB007788

Froment, B., McGuire, J. J., Hilst, R. D., Gouédard, P., Roland, E. C., Zhang, H., & Collins, J. A. (2014). Imaging along-strike variations in mechanical properties of the Gofar transform fault, East Pacific Rise. *Journal of Geophysical Research: Solid Earth, 119*(9), 7175-7194. https://doi.org/10.1002/2014JB011270

Galis, M., Pelties, C., Kristek, J., Moczo, P., Ampuero, J. P., & Mai, P. M. (2015). On the initiation of sustained slip-weakening ruptures by localized stresses. *Geophysical Journal International*, *200*(2), 890-909. https://doi.org/10.1093/gji/ggu436

Harris, R. A., & Day, S. M. (1997). Effects of a low-velocity zone on a dynamic rupture. *Bulletin of the Seismological Society of America*, *87*(5), 1267-1280.

Huang, Y., & Ampuero, J. P. (2011). Pulse-like ruptures induced by low-velocity fault zones. *Journal of Geophysical Research: Solid Earth*, *116*, B12307, https://doi.org/10.1029/2011JB008684

Huang, Y., Ampuero, J. P., & Helmberger, D. V. (2014). Earthquake ruptures modulated by waves in damaged fault zones. *Journal of Geophysical Research: Solid Earth*, *119*(4), 3133-3154. https://doi.org/10.1002/2013JB010724

Huang, Y., Ampuero, J. P., & Helmberger, D. V. (2016). The potential for supershear earthquakes in damaged fault zones–theory and observations. *Earth and Planetary Science Letters*, *433*, 109-115. https://doi.org/10.1016/j.epsl.2015.10.046

Jolivet, R., Bürgmann, R., & Houlié, N. (2009). Geodetic exploration of the elastic properties across and within the northern San Andreas Fault zone. *Earth and Planetary Science Letters*, *288*(1-2), 126-131. https://doi.org/10.1016/j.epsl.2009.09.014.

Kame, N., Saito, S., & Oguni, K. (2008). Quasi-static analysis of strike fault growth in layered media. *Geophysical Journal International, 173*(1), 309-314. https://doi.org/10.1111/j.1365-246X.2008.03728.x

Kammer, D. S., Radiguet, M., Ampuero, J. P., & Molinari, J. F. (2015). Linear elastic fracture mechanics predicts the propagation distance of frictional slip. *Tribology letters, 57*(3), 23. https://doi.org/10.1007/s11249-014-0451-8

Kaneko, Y., Ampuero, J. P., & Lapusta, N. (2011). Spectral-element simulations of long-term fault slip: Effect of low-rigidity layers on earthquake-cycle dynamics. *Journal of Geophysical Research: Solid Earth, 116*(B10). https://doi.org/10.1029/2011JB008395

Lapusta, N., Rice, J. R., Ben-Zion, Y., & Zheng, G. (2000). Elastodynamic analysis for slow tectonic loading with spontaneous rupture episodes on faults with rate-and state-dependent friction. *Journal of Geophysical Research: Solid Earth, 105*(B10), 23765-23789. https://doi.org/10.1029/2000JB900250

Lewis, M. A., & Ben-Zion, Y. (2010). Diversity of fault zone damage and trapping structures in the Parkfield section of the San Andreas Fault from comprehensive analysis of near fault seismograms. *Geophysical Journal International*, *183*(3), 1579-1595. https://doi.org/10.1111/j.1365-246X.2010.04816.x.

Li, H., Zhu, L., & Yang, H. (2007). High-resolution structures of the Landers fault zone inferred from aftershock waveform data. *Geophysical Journal International*, *171*(3), 1295-1307. https://doi.org/10.1111/j.1365-246X.2007.03608.x.

Li, Y. G., Aki, K., Adams, D., Hasemi, A., & Lee, W. H. (1994). Seismic guided waves trapped in the fault zone of the Landers, California, earthquake of 1992. *Journal of Geophysical Research: Solid Earth*, *99*(B6), 11705-11722.

Ma, X. & Elbanna, A.E. (2015). Effect of off-fault low-velocity elastic inclusions on supershear rupture dynamics. *Geophysical Journal International, 203*(1), 664-677. https://doi.org/10.1093/gji/ggv302

Materna K., & Bu☐rgmann, R. (2016). Constraints in compliant fault zone properties inferred from geodetic measurements in the San Francisco Bay area. *Journal of Geophysical Research: Solid Earth*, **121**, 6916-6931. https://doi.org/10.1002/2016JB013243

Mitchell, T. M., & Faulkner, D. R. (2009). The nature and origin of off-fault damage surrounding strike-slip fault zones with a wide range of displacements: A field study from the Atacama fault system, northern Chile. *Journal of Structural Geology, 31*(8), 802-816. https://doi.org/10.1016/j.jsg.2009.05.002

Najdahmadi, B., Bohnhoff, M., & Ben-Zion, Y. (2016). Bimaterial interfaces at the Karadere segment of the North Anatolian Fault, northwestern Turkey. *Journal of Geophysical Research: Solid Earth*, *121*(2), 931-950. https://doi.org/10.1002/2015JB012601

Noda, H., Dunham, E. M., & Rice, J. R. (2009). Earthquake ruptures with thermal weakening and the operation of major faults at low overall stress levels. *Journal of Geophysical Research: Solid Earth*, *114*, B07302. https//doi.org/10.1029/2008JB006143

Pelties, C., Huang, Y., & Ampuero, J. P. (2015). Pulse-like rupture induced by three-dimensional fault zone flower structures. *Pure and Applied Geophysics*, *172*(5), 1229-1241. https://doi.org/10.1007/s00024-014-0881-0

Perrin, C., Manighetti, I., Ampuero, J. P., Cappa, F., & Gaudemer, Y. (2016). Location of largest earthquake slip and fast rupture controlled by along-strike change in fault structural maturity due to fault growth. *Journal of Geophysical Research: Solid Earth*, *121*(5), 3666-3685. https://doi.org/10.1002/2015JB012671

Powers, P. M., & Jordan, T. H. (2010). Distribution of seismicity across strike‐slip faults in California. *Journal of Geophysical Research: Solid Earth*, *115*, B05305. https://doi.org/10.1029/2008JB006234

Qiu, H., Ben-Zion, Y., Ross, Z. E., Share, P. E., & Vernon, F. L. (2017). Internal structure of the San Jacinto fault zone at Jackass Flat from data recorded by a dense linear array. *Geophysical Journal International*, *209*(3), 1369-1388. https://doi.org/10.1093/gji/ggx096

Rice, J. R. (1992). Fault stress states, pore pressure distributions, and the weakness of the San Andreas fault. *International Geophysics*, *51,* 475-503. https://doi.org/10.1016/S0074-6142(08)62835-1

Rice, J. R. (1993). Spatio-temporal complexity of slip on a fault. *Journal of Geophysical Research: Solid Earth,* *98*(B6), 9885-9907. https://doi.org/10.1029/93JB00191

Rice, J. R., Sammis, C. G., & Parsons, R. (2005). Off-fault secondary failure induced by a dynamic slip pulse. *Bulletin of the Seismological Society of America, 95*(1), 109-134. https://doi.org/10.1785/0120030166

Ross, Z. E., Hauksson, E., & Ben-Zion, Y. (2017). Abundant off-fault seismicity and orthogonal structures in the San Jacinto fault zone. *Science Advances, 3*(3), e1601946.

Rowe, C. D., Moore, J. C., Remitti, F., & IODP Expedition 343/343T Scientists. (2013). The thickness of subduction plate boundary faults from the seafloor into the seismogenic zone. *Geology, 41*(9), 991-994. https://doi.org/10.1130/G34556.1

Rubin, A. M., & Ampuero, J. P. (2005). Earthquake nucleation on (aging) rate and state faults. *Journal of Geophysical Research: Solid Earth, 110*(B11). https://doi.org/10.1029/2005JB003686

Rubin A. M., & Ampuero, J.-P. (2007). Aftershock asymmetry on a biomaterial interface. *Journal of Geophysical Research: Solid Earth*, *112*, B05307, 771-786. https://doi.org/10.1029/2006JB004337

Rybicki, K. R., & Yamashita, T. (2002). On faulting in inhomogeneous media. *Geophysical research letters, 29*(10). https://doi.org/10.1029/2002GL014672

Sanders, C. O., & Kanamori, H. (1984). A seismotectonic analysis of the Anza seismic gap, San Jacinto fault zone, southern California. *Journal of Geophysical Research: Solid Earth*, *89*(B7), 5873-5890. https://doi.org/10.1029/JB089iB07p05873

Savage, H. M., & Brodsky, E. E. (2011). Collateral damage: Evolution with displacement of fracture distribution and secondary fault strands in fault damage zones. *Journal of Geophysical Research: Solid Earth*, *116*(B3). https://doi.org/10.1029/2010JB007665

Share, P. E., & Ben-Zion, Y. (2016). Bimaterial interfaces in the South San Andreas Fault with opposite velocity contrasts NW and SE from San Gorgonio Pass. *Geophysical Research Letters*, *43*(20). https://doi.org/10.1002/2016GL070774

Smith, D. E., & Heaton, T. H. (2011). Models of stochastic, spatially varying stress in the crust compatible with focal-mechanism data, and how stress inversions can be biased toward the stress rate. *Bulletin of the Seismological Society of America*, *101*(3), 1396-1421. https://doi.org/10.1785/0120100058

Spudich, P., & Olsen, K. B. (2001). Fault zone amplified waves as a possible seismic hazard along the Calaveras fault in central California. *Geophysical Research Letters*, *28*(13), 2533-2536. https://doi.org/10.1029/2000GL011902

Tada, H., Paris, P. C., & Irwin, G. R. (2000). The stress analysis of cracks handbook, 3rd edn. ASME, New York.

Thakur, P., & Huang, Y. (2018). Constraints on spatial distribution of earthquakes within a 2-D damaged fault zone in seismic cycles. *Seismological Research Letters, 89*(2B), 882-883.

Thomas, M. Y., Bhat, H. S., & Klinger, Y. (2017). Effect of Brittle Off-Fault Damage on Earthquake Rupture Dynamics. *Fault Zone Dynamic Processes: Evolution of Fault Properties During Seismic Rupture, 227*, 255-280. https://doi.org/10.1002/9781119156895.ch14

Uenishi, K., & Rice, J. R. (2003). Universal nucleation length for slip-weakening rupture instability under nonuniform fault loading. *Journal of Geophysical Research: Solid Earth*, *108*(B1), 2042. https://doi.org/10.1029/2001JB001681

Weng, H., Yang, H., Zhang, Z., & Chen, X. (2016). Earthquake rupture extents and coseismic slips promoted by damaged fault zones. *Journal of Geophysical Research: Solid Earth, 121*(6), 4446-4457. https://doi.org/10.1002/2015JB012713

Wolfson-Schwehr, M., Boettcher, M. S., McGuire, J. J., & Collins, J. A. (2014). The relationship between seismicity and fault structure on the Discovery transform fault, East Pacific Rise. *Geochemistry, Geophysics, Geosystems, 15*(9), 3698-3712. https://doi.org/10.1002/2014GC005445

Xu, J., Zhang, H., & Chen, X. (2015). Rupture phase diagrams for a planar fault in 3-D full-space and half-space. *Geophysical Journal International, 202*(3), 2194-2206. https://doi.org/10.1093/gji/ggv284

Xu, S., Ben-Zion, Y., Ampuero, J. P., & Lyakhovsky, V. (2015). Dynamic ruptures on a frictional interface with off-fault brittle damage: feedback mechanisms and effects on slip and near-fault motion. *Pure and Applied Geophysics, 172*(5), 1243-1267. https://doi.org/10.1007/s00024-014-0923-7

Yang, H., & Zhu, L. (2010). Shallow low-velocity zone of the San Jacinto fault from local earthquake waveform modelling. *Geophysical Journal International*, *183*(1), 421-432. https://doi.org/10.1111/j.1365-246X.2010.04744.x.

Yang, H., Li, Z., Peng, Z., Ben-Zion, Y., & Vernon, F. (2014). Low-velocity zones along the San Jacinto Fault, Southern California, from body waves recorded in dense linear arrays. *Journal of Geophysical Research: Solid Earth*, *119*(12), 8976-8990. https://doi.org/10.1002/2014JB011548

Zoback, M., Hickman, S., Ellsworth, W. & the SAFOD Science Team (2011). Scientific drilling into the San Andreas fault zone–an overview of SAFOD's first five years. *Scientific Drilling, 11*, 14-28. https://doi.org/10.2204/iodp.sd.11.02.2011

Figure captions

Figure 1. The setup of the 2D dynamic in-plane rupture model viewed from a cross section in the along-strike direction (x axis) and the fault-normal direction (z axis). The magenta star denotes

the hypocenter. Rupture is nucleated in the damaged fault zone and propagates on a preexisting fault towards the zone of intact rocks in the along-strike direction. The initial shear stress and normal stress are denoted as τ_0 and σ_0, respectively. Note that the initial stresses can be either uniform or heterogeneous in the along-strike direction. The computation domain has absorbing boundaries at the edges to avoid artificial wave reflections.

Figure 2. The off-fault distribution of shear wave velocities for different types of damaged fault zones viewed from cross sections in the along-strike direction and the fault-normal direction. The magenta star denotes the hypocenter of the modeled rupture. The fault is at $z = 0$ and extends through the damaged fault zone and the zone of intact rocks. Only a quadrant of the medium is shown for (a), (b) and (c) because of the fault zone symmetry. Rupture is allowed to propagate bilaterally in all four cases.

Figure 3. Top: Slip rate function of in-plane rupture (a) in a homogeneous medium when the nucleation half-length is 1 L_c and (b) in a 1 L_c wide sharp fault zone with 50% velocity reduction when the nucleation half-length is 0.4 L_c. The slip rate is plotted at time intervals of 2 t_c. The bottom panel shows rupture speeds normalized by the shear wave velocity of the host rock.

Figure 4. Top: Slip rate function of in-plane rupture nucleated in 1 L_c wide sharp fault zones with 50% velocity reduction that end at a distance of (a) 4 L_c and (b) 5 L_c from the hypocenter when the nucleation half-length is 0.6 L_c. The slip rate is plotted at time intervals of 1 t_c. The bottom panel shows rupture speeds normalized by the shear wave velocity of the host rock.

Figure 5. Conditions that lead to rupture arrest (cross) and continuing rupture propagation (square) in sharp (blue) and smooth fault zones (yellow) with different widths when the nucleation half-length is 0.4 L_c. The fault zones have 50% velocity reduction at the fault. The dashed lines show the inferred boundaries between the two types of conditions based on ~90 rupture simulations.

Figure 6. Top: Slip rate function of in-plane rupture nucleated in 2 L_c wide rough fault zones ($l_z = 1\ L_c$ and $l_x = 0.165\ L_c$) with 50% velocity reduction that have a roughness α of (a) 0.5 and (b) 0.2 when the nucleation half-length is 0.6 L_c. The rough fault zones end at a distance of 4
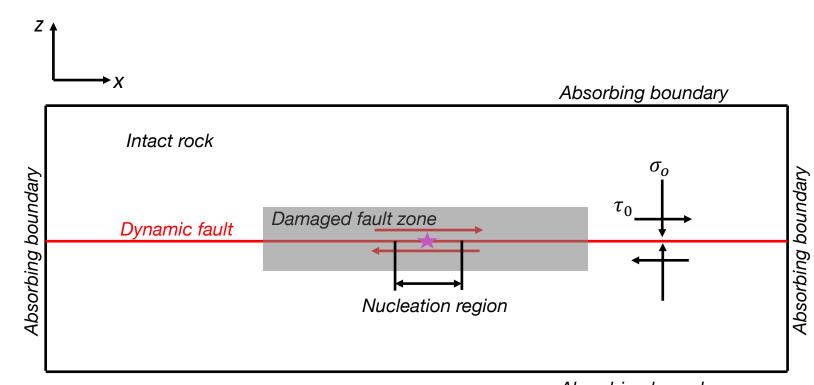
L_c from the hypocenter. The slip rate is plotted at time intervals of 1 t_c. Figure 2c shows the off-fault distribution of shear wave velocities for the case (b). The bottom panel shows rupture speeds normalized by the shear wave velocity of the host rock.
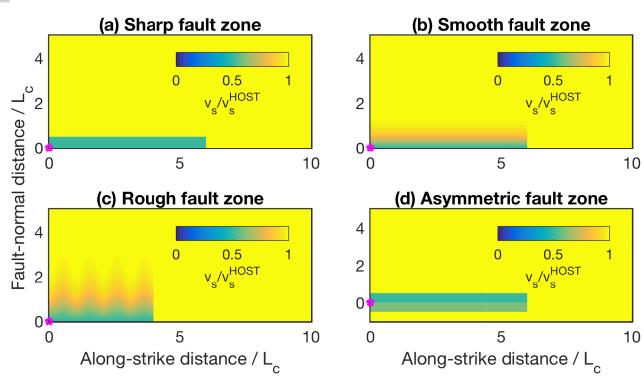
Figure 7. Slip rate function of in-plane rupture nucleated in a 1 L_c wide asymmetric fault zone with 50% velocity reduction in the top layer and 40% velocity reduction in the bottom layer when the nucleation half-length is 0.6 L_c. The asymmetric fault zones end at a distance of (a) 4 L_c and (b) 6 L_c (bottom) from the hypocenter. The slip rate is plotted at time intervals of 1 t_c. Figure 2d shows the off-fault distribution of shear wave velocities for the case (b).
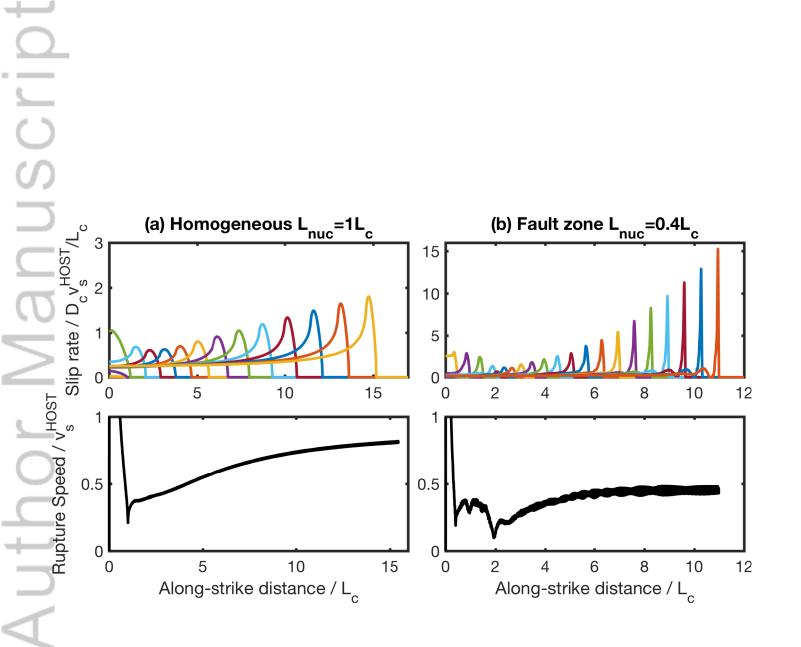
Figure 8. The critical shear stress conditions (black line) that allow in-plane rupture with a nucleation half-length of 0.4 L_c to penetrate into the zone of intact rocks and the resulting rupture speeds (blue line) for the cases of (a) uniformly higher shear stress and of (b) a localized shear stress asperity in the zone of intact rocks (gray). The 1 L_c wide sharp fault zone with 50% velocity reduction ends at a distance of 6 L_c from the hypocenter. Rupture would stop near the zone of intact rocks if initial shear stresses in the intact rocks were lower than the critical conditions.

Figure 9. Top: Slip rate function of anti-plane rupture nucleated in 1 L_c wide sharp fault zones with 50% velocity reduction that end at a distance of (a) 3 L_c and (b) 4 L_c from the hypocenter when the nucleation half-length is 0.4 L_c. The slip rate is plotted at time intervals of 1 t_c. The bottom panel shows rupture speeds normalized by the shear wave velocity of the host rock.

(a) Sharp fault zone

(b) Smooth fault zone

(c) Rough fault zone

(d) Asymmetric fault zone

Fault-normal distance / L_c

Along-strike distance / L_c

v_s/v_s^{HOST}

(a) Homogeneous $L_{nuc}=1L_c$

(b) Fault zone $L_{nuc}=0.4L_c$

Slip rate / $D_c v_s^{HOST}/L_c$

Rupture Speed / v_s^{HOST}

Along-strike distance / L_c

(a) Fault zone ends at $4L_c$

(b) Fault zone ends at $5L_c$

Slip rate / $D_c v_s^{HOST}/L_c$

Rupture Speed / v_s^{HOST}

Along-strike distance / L_c

(a) Rough fault zone $\alpha=0.5$

(b) Rough fault zone $\alpha=0.2$

Slip rate / $D_c v_s^{HOST}/L_c$

Rupture Speed / v_s^{HOST}

Along-strike distance / L_c

(a) Asymmetric fault zone ends at -4 L_c and 4 L_c

(b) Asymmetric fault zone ends at -6 L_c and 6 L_c

Along-strike distance / Lc

(a) Uniformly higher shear stress in the zone of intact rocks

(b) A localized shear stress asperity in the zone of intact rocks

(a) Fault zone ends at 3L_c (anti-plane)

(b) Fault zone ends at 4L_c (anti-plane)